Aharonov-Bohm-effect induced transparency and reflection in mesoscopic rings side coupled to a quantum wire

T. Mrabti, Z. Labdouti, A. Mouadili, E.H. El Boudouti, Bahram Djafari-Rouhani

Aharonov-Bohm-effect induced transparency and reflection in mesoscopic rings side coupled to a quantum wire

T. Mrabti [a], Z. Labdouti [b], A. Mouadili [c], E.H. El Boudouti [b,*], B. Djafari-Rouhani [d]

[a] LSTA, Département de Physique, Faculté Polydisciplinaire de Larache, Université Abdemalek Essaadi, Tétouan, Morocco
[b] LPMR, Département de Physique, Faculté des Sciences, Université Mohammed I, Oujda, Morocco
[c] LPMCER, Département de Physique, Faculté des Sciences et Techniques de Mohammedia, Université Hassan II, Casablanca, Morocco
[d] IEMN, UMR CNRS 8520, Département de Physique, Université de Lille, 59655, Villeneuve d'Ascq, France

We demonstrate analytically and numerically the possibility of existence of the analogues of electromagnetic induced transparency (EIT) and electromagnetic induced reflection (EIR) in a simple mesoscopic structure. The latter consists of a ring of length $2d$ attached vertically to two semi-infinite leads (waveguide) by a wire of length d_1. The ring is threaded by a magnetic flux Φ, the so-called Aharonov-Bohm effect. The number of dangling wire- ring resonators attached at the same point can be increased to N. First, we demonstrate analytically that in the absence of the magnetic flux ($\Phi = 0$) and for particular values of d_1, the structure may present some states that are confined in the ring and do not interact with the waveguide states. These trapped states fall in the continuum states of the two leads and therefore represent bound in continuum (BIC) states. These states are characterized by a zero width resonance (i.e., infinite life-time) in the transmission and reflection spectra. In presence of a weak magnetic flux ($\Phi \neq 0$), the BIC states transform to EIT or EIR resonances for specific values of the lengths $d_1$and d of the wire and the ring respectively. In addition to the numerical results, we have developed Taylor expansion calculations of the transmission and reflection coefficients around EIT and EIR resonances to show that the latter can be written following a Fano shape. In particular, we have deduced the Fano parameter q and the quality factor Q of these resonances as function of N and the flux Φ. We have found that Q decreases as function of Φ for both EIT and EIR resonances, whereas it increases (decreases) as function of N for EIT (EIR) resonances. These results show the possibility of tuning EIT and EIR resonances by means of the magnetic flux Φ and the number of dangling resonators N. The effect of temperature on EIT and EIR resonances is also considered through an analysis of the Landauer-Buttiker conductance formula obtained from transmission. The theoretical results are obtained within the framework of the Green's function method which enables us to deduce analytically the dispersion relation, transmission and reflection coefficients. These results may have important applications for electronic transport in mesoscopic systems such as filters and demultiplexers.

1. Introduction

Electromagnetically induced transparency (EIT) is a quantum interference phenomenon resulting from coherent interactions between the excitation pathways to the atomic upper levels [1,2]. This phenomenon which can turn an opaque system into a transparent system was first observed in Strontium vapor by Boller at al [1]. This resonance is characterized by a dip inserted between two peaks in the absorption followed by a steep dispersion [2]. The EIT-like behavior has received increasing attention during the last two decades, due to its interesting physics and potential applications such as slow light effect [3–5] and data storage [6]. Recent studies have demonstrated that the analog of EIT can be also realized in classical systems due to similar interference effects. Different systems have been proposed for this purpose such as: photonic crystal waveguides coupled to cavities [7–9], coupled-microresonator systems [10,11], nonlinear materials [12,13], plasmonic nanostructures and metamaterials [14,15], acoustic waveguides [16–18], multilayers [19] and photonic circuits [20,21]. In addition to the EIT resonances, the electromagnetically induced reflection (EIR) refers to the formation of a reflection window inside a transparency band of an atomic system. Recently, this effect has been studied theoretically [22,23] and experimentally [24] in metamaterials

* Corresponding author.
E-mail address: elboudouti@yahoo.fr (E.H. El Boudouti).

made of wire-slot and split-ring resonator arrays. Other works have treated theoretically [25] and experimentally [26] EIR resonances in planar metamaterials for plasmonic sensing applications. Also, other structures based on graphene plasmonic devices [27], coupled-resonators in photonic-crystal waveguides [28] and metal–insulator–metal plasmonic waveguide-resonator coupling systems [29], have shown EIR resonances. In addition, EIR resonances have been proposed to realize a narrow-band perfect absorber with two absorption peaks for plasmonic sensor [30]. Besides EIT and EIR resonances, bound in continuum (BIC) sates or trapped modes have found an increasing interest in recent years [31]. These states can be found when the EIT and EIR resonances collapse in the transmission and reflection spectra. Therefore, they remain confined in some parts of the system even though they coexist with a continuous spectral range of radiating waves that can transport energy away. This is a counterintuitive idea which was originally proposed several decades before in quantum mechanics [32], but found a high amount of interest in the recent literature [31]. These states may exhibit potential applications as they are characterized by a high quality factor [31].

In the low dimensional systems, a rich variety of mesoscopic systems [33] have been proposed in the literature to understand transport phenomena through quantum rings, wires, or dots due to the advances in micro-fabrication. Indeed, it has been made possible the confinement of electrons in a conductor with ultrasmall lateral extent of few nanometers, leading to the phase coherence length of the electron to become larger than the system's dimensions. As a result, the system becomes essentially an electron waveguide. These nano-devices have shown several nontrivial effects, such as Aharonov–Bohm (A-B) conductance oscillations, persistent currents and quantum Hall effect [34]. The A-B effect is one of the most intriguing quantum mechanical phenomenon in which the phase of a charged particle is affected by the vector potential of an electromagnetic field giving rise to charge–particle interference phenomena [35,36]. This effect has found applications in different domains such as: electron phase spectroscopy [37], detection of single-molecule levels [38,39], and characterization of nanostructures such as graphene nanotubes [40,41]. This phenomenon has been extended recently to classical photonic structures based on transitions between two photonic modes [42,43] as well as photon-phonon interaction [44]. Different geometrical mesoscopic devices have been explored in the literature to show essentially another type of resonances called Fano resonances [45,46]. These latter resonances are characterized by a peak followed by a dip in the transmission spectra as a consequence of a destructive interference of the waves, giving rise to an asymmetric line shape. These resonances have been the subject of intensive study from the theoretical and experimental point of view in single [47–57] and double [58–65] rings placed between two leads. In addition to Fano resonances, persistent currents are also studied in detail in A-B structures made of one or double rings [47,53,58] in presence of the magnetic flux and impurity or quantum dots in the arms of the ring. However, few works have been devoted to EIT resonances in mesoscopic systems. Some of us [57] have studied a one-dimensional loop structure with dangling resonators on both sides. EIT-like resonances have been obtained by tailoring the lengths of the different wires constituting this structure. A resonance squeezed between two transmission zeros has been also found in a double quantum-ring [66] and a double stub cavity [67] connected at the same site along a quantum wire. Also, to our knowledge, EIR resonances in mesoscopic systems have not been treated before.

In this work, we propose a simple and compact mesoscopic structure that enables to support BIC states, as well as EIT and EIR resonances. The system is composed of a ring of length 2*d*attached vertically to two semi-infinite leads (waveguide) by a wire of length d_1. The ring is threaded by a magnetic flux Φ the so-called Aharonov-Bohm effect. The number of dangling wire-ring resonators attached at the same point is N (Fig. 1). We show that such a structure may exhibit trapped states as well as EIT and EIR resonances that can be tuned by means of the magnetic flux Φ and the number of dangling resonators *N*.

The effect of temperature on EIT and EIR resonances is also considered through an analysis of the Landauer-Buttiker conductance from transmission formula [68,69]. The theoretical results are obtained within the framework of the Green's function method [70] which enables us to deduce the dispersion relation and transmission and reflection coefficients.

This paper is organized as follows: in Sec. 2 we recall the Green's functions expressions of the wire, ring and leads constituting the whole structure (Fig. 1). Then, we show how to deduce the expressions of the transmission and reflection coefficients. Section 3 is devoted to analytical and numerical results of transmission and reflection coefficients to show the possibility of existence of BIC, EIT and EIR resonances. The effect of temperature on EIT and EIR resonances is discussed in Sec. 4. Section 5 gives a summary of the main results of this work and the conclusion.

2. Theoretical results: transmission and reflection coefficients and dispersion relations

2.1. Green's functions approach

The mesoscopic structure described in Fig. 1 is composed of *N* mesoscopic Aharonov- Bohm rings of length 2*d* attached to a wire of length d_1, all the rings are threaded by the same magnetic flux Φ. The whole structure is inserted between two semi-infinite leads. We use the Green's function approach, called interface response theory of continuous media [70] to solve the problem of the propagation of electronic waves in the structure presented in this work (Fig (1)). The objective of this theory is to calculate the Green's function of a composite system containing a large number of interfaces that separate different homogenous media. The knowledge of this Green's function enables us to obtain different physical properties of the system such as the reflection and transmission coefficients and the dispersion relations. All the matrix elements g(DD) in the whole space D of the composite material, can be obtained from the knowledge of the matrix elements $g(MM)$ in the interface space M. $g(MM)$ is calculated from its inverse $g^{-1}(MM)$. The latter is formed by a linear superposition of the surface matrix elements $g_i^{-1}(MM)$ of any independent wire [70]. We employ the usual boundary conditions: the continuity of the wave functions and their first derivatives divided by the respective effective masses. These are implicitly taken into account in the framework of Interface Response Theory [70].

We shall avoid the details of calculation where an analysis of the Shrödinger equation in presence of a magnetic flux gives rise to the bulk Green's function of an infinite wire. These calculations are presented

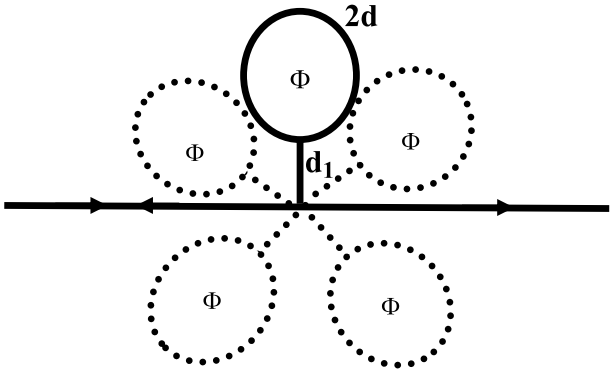

Fig. 1. Schematic illustration of N ($N = 5$) Aharonov-Bohm rings of length 2*d* coupled to the waveguide by a wire of length d_1, the rings are threaded by a magnetic flux Φ. The whole structure is inserted between two semi-infinite leads.

elsewhere [65].

The principle of the interface response theory [70] used in this work, requires before dealing with the whole structure, the knowledge of the surface Green's functions elements of its elementary constituents, namely, the Green's function of a finite wire of length d_1 and of an Aharonov-Bohm ring of length $2d$ submitted to a magnetic flux Φ. The inverse of the Green's function $g_1^{-1}(M_1M_1)$ in the space of interface $M_1 = \{0,1\}$ of a finite wire of length d_1 (Fig. 2(a)) can be written as a (2×2) matrix [65]:

$$g_w^{-1}(M_1M_1) = -F\begin{pmatrix} \frac{C_1}{S_1} & \frac{-1}{S_1} \\ \frac{-1}{S_1} & \frac{C_1}{S1} \end{pmatrix} \tag{1}$$

where $S_1 = \sin(kd_1)$, $C_1 = \cos(kd_1)$ and $F = (\hbar^2/2m)k$ and $k = \sqrt{2mE}/\hbar$. $\hbar$, k and m refer respectively to the reduced Planck constant, the wave vector of the constituting medium and the effective mass of the electron. The inverse of the Green's function $g_r^{-1}(M_2M_2)$ in the space of interface $M_2 = \{1,2\}$ of the ring made of two wires of length d and in presence of a magnetic flux Φ (Fig. 2(b)) can be written as a (2×2) matrix, namely [65].

$$g_r^{-1}(M_2M_2) = -F\begin{pmatrix} \frac{2C}{S} & \frac{-2C'}{S} \\ \frac{-2C'}{S} & \frac{2C}{S} \end{pmatrix} \tag{2}$$

where $S = \sin(kd)$, $C = \cos(kd)$, $C' = \cos(\pi f)$ and $f = \Phi/\Phi_0$ is the ratio of the flux Φ to the quantum flux Φ_0. $\Phi_0 = h/e$ is the quantum flux associated with a single charge of the electron e. Note that the magnetic field is applied only inside the ring.

The inverse of the Green's function of the wire-ring system (Fig. 3) within the interface space $M = \{0,1,2\}$, is obtained from a juxtaposition of the inverse Green's functions of the two subsystems (Eqs. (1) and (2)) [70], namely

$$g_{w,r}^{-1}(MM) = -F\begin{pmatrix} \frac{C_1}{S_1} & -\frac{1}{S_1} & 0 \\ -\frac{1}{S_1} & \frac{C_1}{S_1}+\frac{2C}{S} & \frac{-2C'}{S} \\ 0 & \frac{-2C'}{S} & \frac{2C}{S} \end{pmatrix} \tag{3}$$

2.2. Transmission and reflection coefficients

In order to calculate the transmission and reflection coefficients through the whole structure depicted in Fig. 1, we need i) the element $g_{w,r}(0,0)$ of the wire-ring system, this element is obtained by inverting the matrix in Eq. (3) and truncating the first element such that

$$g_{w,r}(0,0) = -\frac{1}{2F}\frac{\tau}{\rho} \tag{4}$$

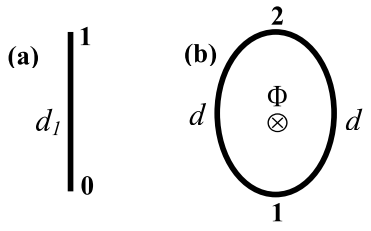

Fig. 2. (a) Schematic illustration of a one-dimensional mesoscopic wire of length d_1 and (b) a mesoscopic ring of length $2d$ threaded by the magnetic flux Φ. The interface space of the wire (a) and ring (b) are called $M_1 = \{0,1\}$ and $M_2 = \{1,2\}$ respectively.

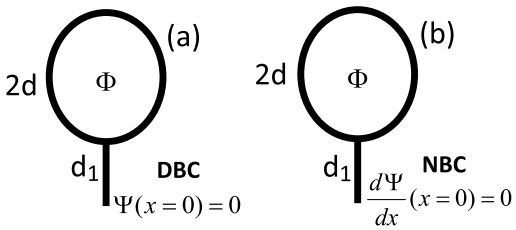

Fig. 3. Ring attached to a wire (ring-wire structure) with Dirichlet (a) and Neumann (b) boundary conditions at the bottom side of the structure.

and ii) the Green's function of the two semi-infinite leads in the space of interface $M_3 = \{0\}$, which is given by Ref. [65].

$$g_s^{-1}(0,0) = 2jF \tag{5}$$

where

$$\tau = 2\left[C_1CS - 2S_1\left(S^2 - S'^2\right)\right],\quad \rho = -\left[CSS_1 + 2C_1\left(S^2 - S'^2\right)\right] \tag{6}$$

$S' = \sin(\pi f)$ and $j = \sqrt{-1}$.

Therefore, the inverse of the Green's function of the whole system (Fig. 1) at the connection point $M_3 = \{0\}$ is given by $g^{-1}(0,0) = Ng_{w,r}^{-1}(0,0) + g_s^{-1}(0,0) = -2NF\frac{\rho}{\tau} + 2jF$.

The transmission coefficient through the structure given in Fig. 1 is defined by Ref. [65] $t = 2jFg(0,0)$. One obtains

$$t = \frac{-j\tau}{N\rho - j\tau} \tag{7}$$

By the same way, the reflection coefficient is given by Ref. [65] $r = -1 + 2jFg(0,0)$, or equivalently

$$r = \frac{-N\rho}{N\rho - j\tau} \tag{8}$$

From the expressions of t (Eq. (8)) and r (Eq. (9)), one can deduce the transmission and reflection rates

$$T = \frac{\tau^2}{\tau^2 + (N\rho)^2} \tag{9}$$

$$R = \frac{(N\rho)^2}{(N\rho)^2 + \tau^2} \tag{10}$$

One can deduce easily from Eqs. (9) and (10) the conservation energy, namely $R + T = 1$.

2.3. Dispersion relations of wire-ring structures with different boundary conditions

The eigenstates of the finite structure made by the wire-ring (Fig. 3), depend on the particular choice of the boundary condition at the bottom side of the wire (Fig. 3). We chose the two most common boundary conditions, namely the vanishing of the wave function (Fig. 3(a)) called *Dirichlet boundary condition* DBC, or of its first derivative (Fig. 3(b)) called *Neumann boundary condition* NBC. Indeed, the eigenstates of the DBC structure (Fig. 3(a)) are given by vanishing the Green's function $g_{w,r}(0,0)$ (Eq. (4)), namely

$$\tau = 0 \tag{11}$$

whereas, the eigenstates of the NBC structure (Fig. 3(b)) are given by the poles of the Green's function $g_{w,r}(0,0)$ (Eq. (4)), namely

$$\rho = 0 \tag{12}$$

The common eigenstates of DBC and NBC structures will appear as trapped or BIC states with respect to the continuum states carried by the

leads (see below). Also, equations (9), (11) and (12) show that the eigenstates of the DBC and NBC structures are directly related respectively to the minima and maxima of the transmission coefficient (Eq. (9)). This property has been used by some of us to deduce both theoretically and experimentally bulk and surface modes [71,72] in coaxial photonic crystals.

3. Numerical results and discussion

3.1. DBC, NBC and BIC states

Before dealing with EIT and EIR resonances through an analysis of the transmission and reflection coefficients (sections 3.2 and 3.3 below), we shall first focus on the analytical and numerical results of the eigenstates in DBC and NBC structures sketched in Fig. (3) as well as the BIC states of the whole structure given in Fig. 1. As mentioned above, the dispersion relations of the ring-wire structure (Fig. 3) with either DBC (Fig. 3(a)) or NBC (Fig. 3(b)) boundary conditions are given by Eqs. (11) and (12) respectively. Therefore, the explicit expressions giving the eigenstates for DBC and NBC structures can be written respectively as

$$S\left[S-\frac{CC_1}{2S_1}\right]-S'^2=0 \tag{13}$$

and

$$S\left[S+\frac{CS_1}{2C_1}\right]-S'^2=0 \tag{14}$$

In the presence of a magnetic flux Φ such that $S' = 0$ (i.e., f is integer) and in particular in the absence of the magnetic field, we obtain two types of eigenstates of the DBC structure (Eq. (13)) which are totally decoupled from each other. These states are given by

$$S=0 \tag{15}$$

or

$$S-\frac{CC_1}{2S_1}=0 \tag{16}$$

They are respectively associated to the eigenmodes of the ring alone or the ring-wire system alone. These two types of states coincide with each other for $S = 0$ and $C_1 = 0$, i.e.,

$$d_1/d=(2m+1)/2n \tag{17}$$

where m and n are integers and $n \neq 0$. Equation (13) shows that the eigenstates of the DBC structure are the consequence of the coupling between the states given by $S = 0$ of the ring alone (Fig. 2(b)) and those given by $S-\frac{CC_1}{2S_1}=0$ which are associated to the coupled ring-wire (Fig. 3(a)). This coupling occurs by means of a magnetic flux such that $S' \neq 0$ (i.e., f is non-integer).

Similarly, the eigenstates of the NBC structure which are given by (Eq. (14)) divide into two totally decoupled sets in the absence of a magnetic field and are given by

$$S=0 \tag{18}$$

or

$$S+\frac{CS_1}{2C_1}=0 \tag{19}$$

These two types of states coincide with each other for $S = 0$ and $S_1 = 0$, i.e.,

$$d_1/d=m/n \tag{20}$$

Equation (14) shows that the eigenstates of the NBC structure are the consequence of the coupling between the states given by $S = 0$ of the ring alone (Fig. 2(b)) and those given by $S+\frac{CS_1}{2C_1}=0$ of the coupled ring-wire (Fig. 3(b)). These results demonstrate that the eigenstates of DBC and NBC structures are the consequence of the coupling between the states of two resonators through the flux created by the magnetic field such that $S' \neq 0$.

The above analysis shows that the states given by $S = 0$ are common to both structures (DBC and NBC). These states are independent of the wire of length d_1 and therefore, in the presence of the magnetic field such that $S' = 0$, they remain trapped in the ring even if the ring-wire structure is connected to the semi-infinite leads. Indeed, the eigenstates of the whole system (Fig. 1) are given by the poles of the Green's function or equivalently the transmission coefficient (Eq. (7)), namely

$$N\rho - j\tau = 0 \tag{21}$$

where$\rho$and τ are given by Eq. (6). This latter equation is a complex quantity. Its real part gives the position of the resonances in the transmission and DOS, whereas its imaginary part is related to the width of the resonances (see below). When the ring is not threaded by a magnetic flux (i.e., f = 0), then using Eq. (6), one can factorize Eq. (21) by the term S as follows

$$S[2(C_1C-2S_1S)-jN(CS_1+2C_1S)]=0 \tag{22}$$

Equation (22) clearly shows that if

$$S=0 \tag{23}$$

(i.e., $C = \pm 1$), then one obtains the eigenstates of the whole system (Fig. 1) even though these states fall in the continuum states of the two semi-infinite leads surrounding the ring-wire structure. These kinds of states are known as bound in continuum (BIC) states [31]. From Eq. (23), BIC states are given by $kd = n\pi$ (n is an integer). The above results show that BIC states are independent of the nature of the boundary condition at the bottom side of the ring-wire structure (Fig. 3), that is why they are common states to DBC and NBC structures and remain totally decoupled from the waveguide on which they are grafted.

In presence of a magnetic flux such that $S' \approx 0$(i.e., f ≈ $l$where l is an integer), we can easily show that it is not possible to cancel simultaneously real and imaginary parts of Eq. (21) at the same energy, which means the impossibility of existence of BIC states. Also, as mentioned above, the eigenstates of the DBC structure (Eqs. (15) and (16)) and NBC structure (Eqs. (18) and (19)) for f = l, become coupled when f ≈ l (see Eqs. (13) and (14)). This coupling between the eigenstates enables to transform the BIC states to either EIT or EIR resonances depending on the length d_1 of the wire as it will be detailed below.

In what follows, we shall first focus on the analytical and numerical results in the case where the structure is composed of a single ring of length 2d in presence of a magnetic flux Φ attached to a wire of length d_1 (i.e, N = 1 in Fig. 1). Also, we shall fix the length 2d of the ring and discuss the effect of the length d_1 of the wire, on the different eigenstates of the system as well as on the transmission and reflection rates. For the sake of simplicity, the length d_1 will be given in units of d (half the length of the ring), and the dimensionless wave vector $\kappa = kd/\pi$ and the magnetic flux $f = \Phi/\Phi_0$ will be used. In addition, we shall focus on the results for a very weak flux (i.e., f ≈ 0) even though the results remain also valid in the case f ≈ l. It is worth mentioning that other possibilities of BIC, EIT and EIR resonances can be obtained for $C' \approx 0$ (i.e., f ≈ l' + 1/2where l' is an integer). The equations governing this case are given in Appendix A.

From Eq. (17), DBC branches cross each other at $d_1 = 0.5, 1.5, \ldots$ given respectively by $n = 1$ and $m = 0, 1, \ldots$ whereas from Eq. (20), NBC branches cross each other at $d_1 = 0,1, \ldots$given respectively by $n = 1$ and $m = 0, 1, \ldots$ Higher energy crossing branches where BIC, EIT and EIR resonances may occur, are given by $n = 2$ (i.e., $kd = 2\pi$) and $m = 0, 1, \ldots$ in Eqs. (17) and (20) and so one. In what follows, we shall concentrate on the case n = 1. Fig. 4(a) gives the dispersion curves of the eigenstates (κ versus d_1) of the DBC structure (dots) and the NBC structure (circles) when no magnetic flux is applied through the ring ($f = 0$). These

dispersion curves are obtained from Eqs. (15), (16) and (19) and plotted in the domain $0 \leq d_1 \leq 1.5$around $\kappa = 1$ (i.e., $kd = \pi$) where the main phenomena (BIC, EIT and EIR resonances) are predicted. Both types of states in Fig. 4(a) exhibit a common horizontal branch at $\kappa = 1$ as predicted from Eqs. (15), (18) and (23). In presence of the magnetic flux (Fig. 4(b)), we assist to a lifting of degeneracy at the crossing points around $d_1 = 0.5,\ 1.5,\ldots$for the DBC structure (blue dots in Fig. 4(b)) and around $d_1 = 0,\ 1,\ldots$ for the NBC structure (red circles in Fig. 4(b)). Indeed, by increasing the magnetic flux, the strength of the separation between the states increases around the anti-crossing points as it is illustrated in Fig. 5(a) and (b) around $d_1 = 0.5$ and $d_1 = 1$for the DBC and NBC structures respectively. Indeed, one can show (see below) that this separation is proportional to the flux f as$\Delta\kappa = \frac{4}{\sqrt{5}}$f at $d_1 = 0.5$for the DBC structure and $\Delta\kappa = \frac{4}{\sqrt{6}}$f at $d_1 = 1$for the NBC structure.

As mentioned above, the eigenstates of the structures with either DBC or NBC are directly related to the minima and maxima of the transmission coefficient (Eqs. (9), (11), (12)). An interesting point that can be noticed in Fig. 4(b) is the existence of a full transmission (red circles) squeezed between two transmission zeros (blue dots) around$d_1 = 0.5$; this is a characteristic of the transparency (or EIT) resonance. This resonance is symmetrically placed between two transmission zeros for $d_1 = 0.5,\ 1.5$ and becomes asymmetric when $d_1$is slightly shifted from these values (Fig. 4(b)). Similarly, this phenomenon is completely inverted around $d_1 = 0,\ 1$where a transmission zero is inserted between two transmission maxima giving rise to a complete reflection; the so-called *electromagnetic induced reflection* (EIR) (see below).

Fig. 6 gives a better insight about the evolution of DBC (blue dots) and NBC (red circles) eigenstates for integers and half integers values of the length$d_1$around $\kappa = 1$ and for f = 0.03. As mentioned above, these states correspond to transmission and reflection zeros given by $\tau = 0$and$\rho = 0$respectively (Eqs. (6), (9) and (10)). We can clearly see a full transmission (reflection) between two transmissions (reflections) zeros for half integers (integers) values ofd_1; these are characteristics of EIT (EIR) resonances. Also, the separation between the transmission zeros and reflection zeros around $\kappa = 1$ decreases considerably when $d_1$increases (Fig. 6).

3.2. Electromagnetic induced transparency

In this section, we shall discuss the EIT resonances falling around $d_1 = 0.5$and $\kappa = 1$. In Fig. 4, we have highlighted the wave vector regions where complete transmission and complete reflection are achieved. However, in order to give a better insight about the behavior of the transmission rate for different values of κ and d_1, we plot in Fig. 7 the transmission spectra (in color scale) versus κ and $d_1$for f = 0 (Fig. 7(a)) and f = 0.03 (Fig. 7(b)). We have indicated by horizontal dashed line the position of BIC states in Fig. 7(a) for f = 0. These states are hidden and do not give any signature in the transmission spectra as the corresponding resonances have zero width (see below). In particular, one can notice at $\kappa = 1$ a decrease of the transmission from one at $d_1 = 0$ to zero at $d_1 = 0.5$ and back to one at $d_1 = 1$. Indeed, when BIC states hold (i.e., $S = 0$ or $\kappa = n$), the transmission rate (Eq. (9)) becomes

$$T = 4C_1^2/\left(4C_1^2 + NS_1^2\right) \tag{24}$$

which shows that for $\kappa = n$, the transmission rate depends strongly on the value of d_1 and oscillates between 0 and 1 when d_1 increases. The positions of full transparency and full reflection regions in Fig. 7(a) coincide with those in Fig. 4(a). By applying a weak magnetic flux f = 0.03 (Fig. 7(b)), a thin transparency window appears between two minima around$\kappa = 1$and$d_1 = 0.5$. The width of this window increases when increasing the magnetic flux as it will be explained below. Also, contrary to the case f = 0 (Fig. 7(a)), the transmission at $\kappa = 1$ and f≠0 (Fig. 7(b)) increases from zero at $d_1 = 0$ to one at $d_1 = 0.5$ and back to zero at$d_1 = 1$according to the equation

$$T = 4S_1^2/\left(4S_1^2 + NC_1^2\right) \tag{25}$$

Fig. 8 gives three examples of the transmission spectra versus κ with (blue curves) and without (red curves) magnetic flux for different values ofd_1. Fig. 8(b) clearly shows that for $d_1 = 0.5$, applying a magnetic flux induces a symmetric transparency window around $\kappa = 1$ in accordance with Fig. 7(b). For $d_1 = 0.3$ (Fig. 8(a)) and $d_1 = 0.7$ (Fig. 8(c)) slightly different from $d_1 = 0.5$, one obtains an asymmetric EIT resonance. This resonance is a consequence of the coupling between the BIC state induced by the ring (Eq. (15)) and the other states induced by the ring-wire (Eq. (16)). In the following subsections, we shall detail the results of symmetric and asymmetric EIT resonances.

3.2.1. Case of symmetric EIT resonance

In the case where $d_1 = 0.5$ and the rings are threaded by a weak magnetic flux, we can obtain an approximate analytical expression for the transmission function (Eq. (7)) in the vicinity of the transparency resonance. A Taylor expansion around $kd = \pi + \varepsilon$ enables us to write

$$t = jA\frac{\zeta_1\zeta'_1}{\varepsilon + j4\Delta^2/N(1+\Delta^2)} \tag{26}$$

where$\zeta_1 = \left(\varepsilon + \frac{2\Delta}{\sqrt{5}}\right)$, $\zeta'_1 = \left(\varepsilon - \frac{2\Delta}{\sqrt{5}}\right)$, $\Delta = \pi$and $A = 5/N(1+\Delta^2)$.

From Eq. (26), one can show that the transmission rate T can be written following a Fano form [45]:

$$T = A^2\frac{(\varepsilon - q_1\Gamma_1)^2(\varepsilon + q_1\Gamma_1)^2}{\varepsilon^2 + \Gamma_1^2} \tag{27}$$

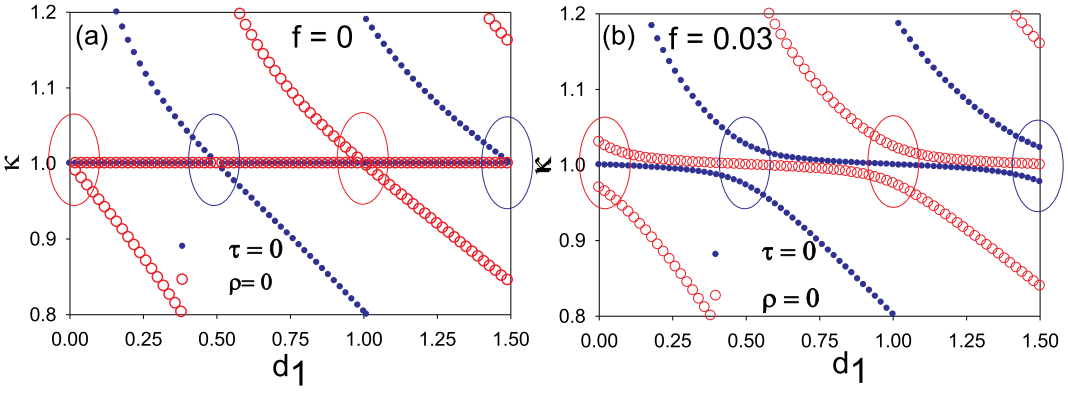

Fig. 4. (a) Dispersion curves of the eigenstates of the structures depicted in Fig. 3(a) with DBC ($\tau = 0$, dots) and Fig. 3(b) with NBC ($\rho = 0$, circles) as a function of the length d_1 for f = 0. (b) Same as in (a) but in the case f = 0.03. The large circles indicate the positions of crossing and anti-crossing branches.

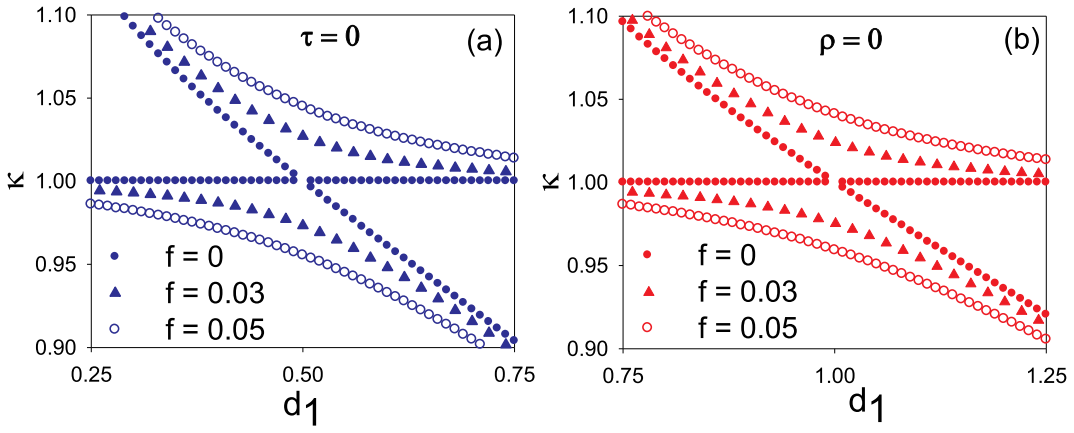

Fig. 5. (a) Zoom of the crossing and anticrossing dispersion curves in Fig. 4 around $d_1 = 0.5$ and$\kappa = 1$for the DBC structure (Fig. 3(a)). (b) Same as in (a) but for the NBC structure around $d_1 = 1$ and $\kappa = 1$. The curves are plotted for three values of the magnetic flux: f = 0 (dots), f = 0.03 (triangles) and f = 0.05 (open circles).

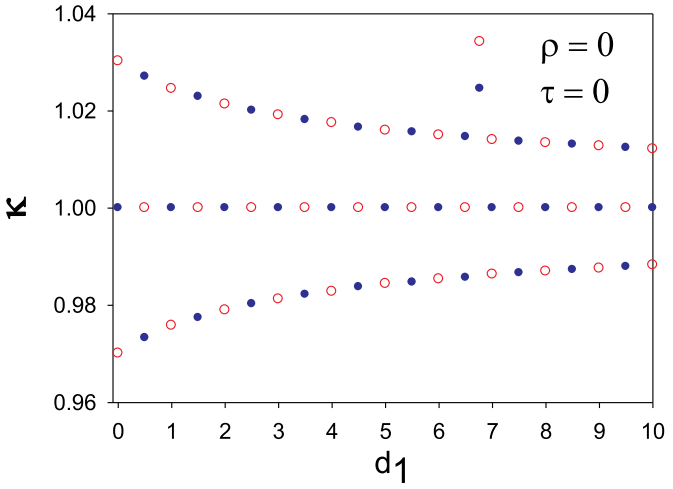

Fig. 6. Transmission zeros (blue dots) and reflection zeros (red circles) as a function of integers and half integers values of the length d_1 around $\kappa = 1$ and for f = 0.03. The transmission and reflection zeros are given by $\tau = 0$and$\rho = 0$respectively (Eqs. (6), (9) and (10)). (For interpretation of the references to color in this figure legend, the reader is referred to the Web version of this article.)

where$q_1 = N(1+\Delta^2)/2\sqrt{5}\Delta$ is the Fano parameter that describes the asymmetry of the resonance. The full width at half maximum of the EIT resonance falling at $\varepsilon = 0$ (i.e., $kd = \pi$), is given by

$$\Gamma_1 = 4\Delta^2/N(1+\Delta^2) \tag{28}$$

and therefore, the quality factor defined by $Q = \pi/\Gamma_1$is given by

$$Q = N\pi(1+\Delta^2)/4\Delta^2 \tag{29}$$

We can notice thatq_1, $\Gamma_1$and Q depend strongly on the magnetic flux f and the number of dangling resonators N. The results of the approximate expression (Eq. (27)) are shown in Fig. 9 by open circles. These results are in accordance with the exact ones (solid lines) and clearly show that the resonance is an EIT-like resonance with $q_1 = 2.37$ and $2\Gamma_1 = 0.068$. This resonance induced magnetically (Aharonov-Bohm effect) is squeezed between two transmission zeros (indicated by solid circles on the abscissa of Fig. 9) located symmetrically around $\kappa = 1$ and reaches unity (i.e., T = 1). The above calculation shows that a simple dangling ring, without introducing any impurity or defect in its arms, enables to obtain an EIT-like resonance with a width $2\Gamma_1$ and a coupling parameter $q_1$that can be tuned easily by varying the magnetic flux.

To discuss the effect of the magnetic flux on the EIT resonance, we have plotted in Fig. 10(a) the transmission coefficient versus the reduced wave vector κ for different values of the magnetic flux. One can notice that when the magnetic flux increases, the width of the EIT resonance increases according to Eq. (28). Also, it is remarkable that the two transmission zeros move symmetrically around $\kappa = 1$ (see the insert of Fig. 10(b)), whereas the amplitude of the EIT resonance remains unity whatever the value of the flux (Fig. 10(a)).

In Fig. 10 (b), we have plotted numerical (solid lines) and approximate (open circles) results of the quality factor Q of the EIT resonance as a function of the magnetic flux f for $N = 1$. The approximate results are obtained from Eq. (29). The exact results are well reproduced by the approximate curve. On the other hand, one can observe that Q decreases when the magnetic flux increases and diverges when the magnetic flux vanishes according to Eq. (29). In the insert of Fig. 10(b), we have plotted by open circles and solid lines the variation of the positions of transmission zeros and EIT resonance versus the magnetic flux f. The slope of the two lines can be obtained easily from the transmission zeros of the approximate expression (Eq. (26)) as$\pm 2/\sqrt{5}$.

In Fig. 11 we study the effect of the parameter N on the resonance transparency and the quality factor.

In Fig. 11(a), we have plotted the transmission coefficient versus the dimensionless wave vector κ for different values of the number N when the magnetic flux is fixed at f = 0.04. These results show that when N increases, the width of the EIT resonance decreases, its amplitudes reaches unity and the positions of the transmission zeros remain constant. The quality factor as a function of N is illustrated in Fig. 11 (b). One can notice that as predicted, Q increases linearly as function of f according to Eq. (29), also with a good agreement between approximate and numerical results.

3.2.2. *Case of asymmetric EIT resonance*

In Fig. 12 (solid line), we have plotted the transmission coefficient versus the dimensionless wave vector κ for different values of $d_1$around $d_1 = 0.5$. The flux is fixed to f = 0.02. Contrary to the previous case where the resonance is squeezed between two symmetric anti-resonances with similar quality factors, the resonances in Fig. 12 exhibit an asymmetric shape. Indeed, without magnetic flux (dashed curves), there exists only one anti-resonance with low Q factor. Turning on the flux, induces a second anti-resonance near $\kappa = 1$ characterized by a high Q factor. Therefore, the EIT resonance around$\kappa = 1$appears as a consequence of the interaction between two resonators with low and high Q factors called dark and bright resonators respectively [73,74]. The bright resonance (low Q) falls at the vicinity of $\kappa = 1$ whatever the value of d_1, whereas the dark resonance (high Q) moves from $\kappa > 1$ for $d_1 < 0.5$ (Fig. 12(a), (b)) to $\kappa < 1$ for $d_1 > 0.5$ (Fig. 12(c), (d)).

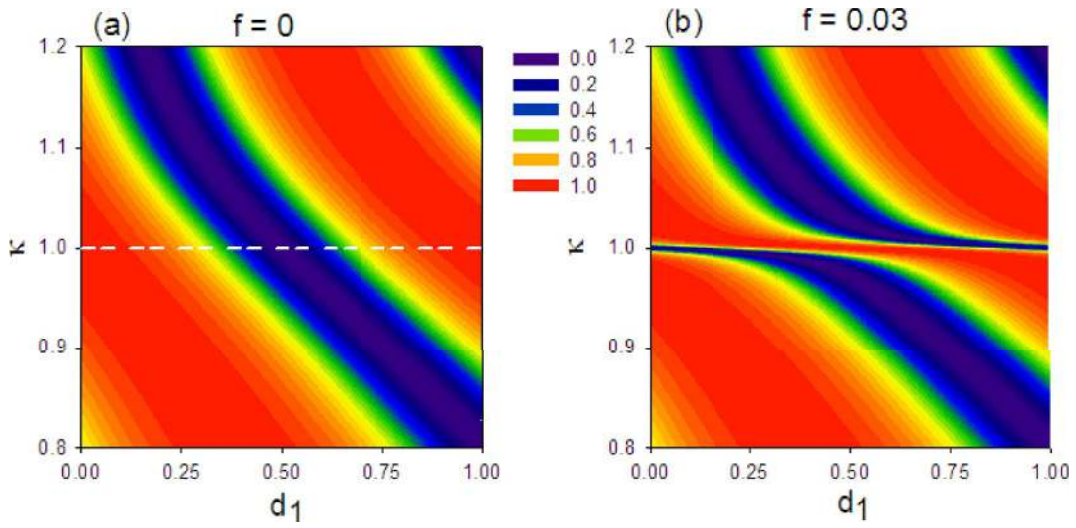

Fig. 7. (a) Transmission spectra (in color scale) versus the dimensionless wave vector κ and the length$d_1$for f = 0. (b) Same as in (a) but for f = 0.03. (For interpretation of the references to color in this figure legend, the reader is referred to the Web version of this article.)

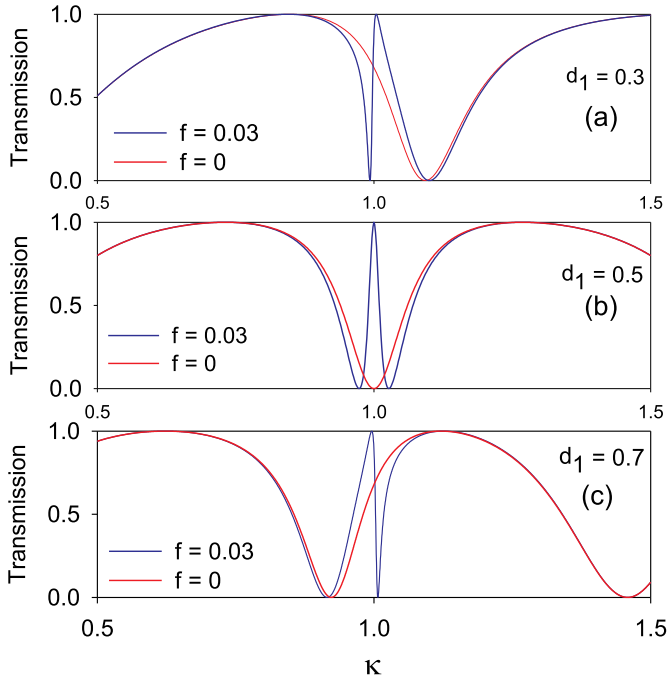

Fig. 8. Transmission cofficient versus the dimensionless wave vector κ for $d_1 = 0.3$ (a), 0.5 (b) and 0.7 (c). The red and blue curves are plotted for f = 0 and 0.03 respectively. (For interpretation of the references to color in this figure legend, the reader is referred to the Web version of this article.)

Similarly to the symmetrical case (section 3.2.1) but with tedious calculation, we can obtain an approximate analytical expression for the transmission function (Eq. (7)) in the vicinity of the transparency resonance. A Taylor expansion around $kd = \pi + \varepsilon$ enables us to write the transmission rate T following a Fano form [45]:

$$T = B\frac{(\varepsilon + q_{1t}\Gamma)^2(\varepsilon + q_{2t}\Gamma)^2}{\varepsilon(\varepsilon - \beta_T) + \Gamma_T^2} \tag{30}$$

where B is a constant. q_{1t} and q_{2t} are the Fano parameters that describe the asymmetry of the resonance. Contrary to the symmetrical case, q_{1t} and q_{2t} are different; their expressions are cumbersome, they depend on the geometrical parameters of the structure as well as on the magnetic

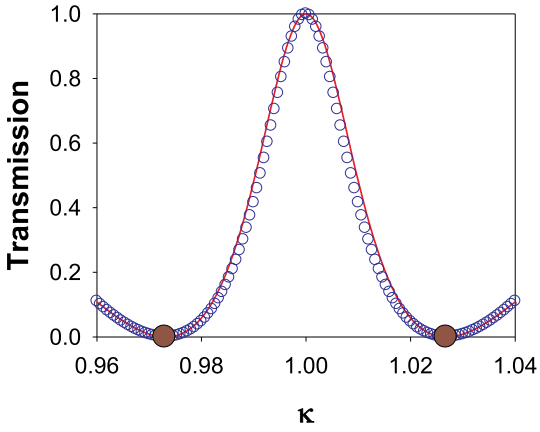

Fig. 9. Transmission spectrum versus κ (solid line) and the approximate results obtained by Taylor expansion (Eq. (27)) (open circles) for the EIT resonance with $d_1 = 0.5$, f = 0.03 and $N = 1$.

flux applied through the rings. We shall avoid giving their expressions here. β_T gives the resonance position; its expression is given by

$$\beta_T = \frac{\Delta^2\phi\left(4 + 4\Delta^2(1+\delta) + N^2\right)\left(2 - \frac{\phi^2}{4}\right)}{N^2\left[(1 + \Delta^2(1+\delta) - \phi^2/8) - \frac{\phi^2}{2}(5+\delta)\right]} \tag{31}$$

The full width at half maximum of the EIT resonance falling at $\varepsilon = \beta_T$, is given by

$$\Gamma_T = \left(\frac{N^2\Delta^4\phi^2 + 4\Delta^4\left(2 - \frac{\phi^2}{4}\right)^2}{N^2\left[\left(1 + \Delta^2\left(1+\delta\right) - \phi^2\Big/8\right) - \frac{\phi^2}{2}\left(5+\delta\right)\right]}\right)^{0.5} \tag{32}$$

where $\Delta = \pi f$, $\phi = \pi\delta$ and $\delta = 2d_1\text{-}d$. Therefore, the quality factor can be deduced as $Q_T = \pi/\Gamma_T$.

The results of the approximate expression (Eq. (30)) are shown in Fig. 12 by red open circles. These results are in accordance with the exact ones (solid lines) and clearly show that the resonance is an asymmetric EIT resonance. This resonance induced magnetically (Aharonov-Bohm effect) is squeezed between two transmission zeros located asymmetrically around κ = 1 and reaches unity (i.e., T = 1)

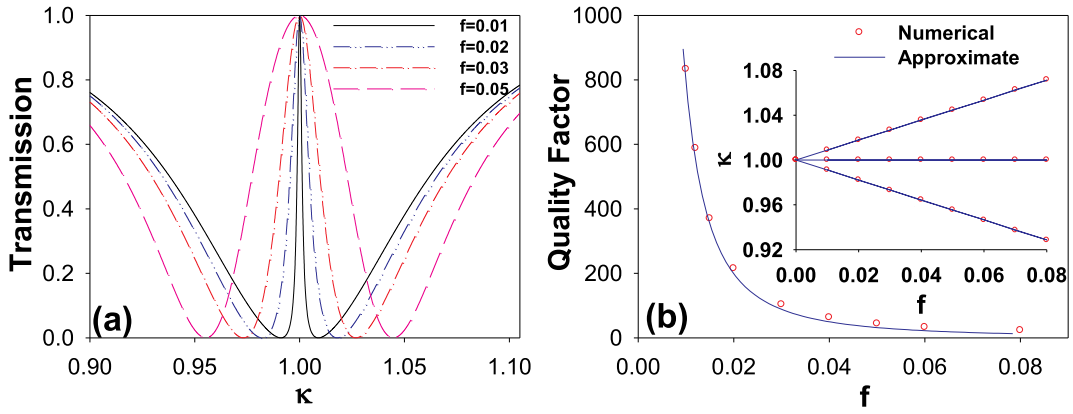

Fig. 10. (a) Same as in Fig. 8 (b) around $\kappa = 1$ and for different values of the magnetic flux. (b) Quality factor versus the magnetic flux f. Solid lines and open circles correspond to numerical and approximate results respectively. The insert shows the variation of the positions of EIT resonance and transmission zeros versus the magnetic flux f.

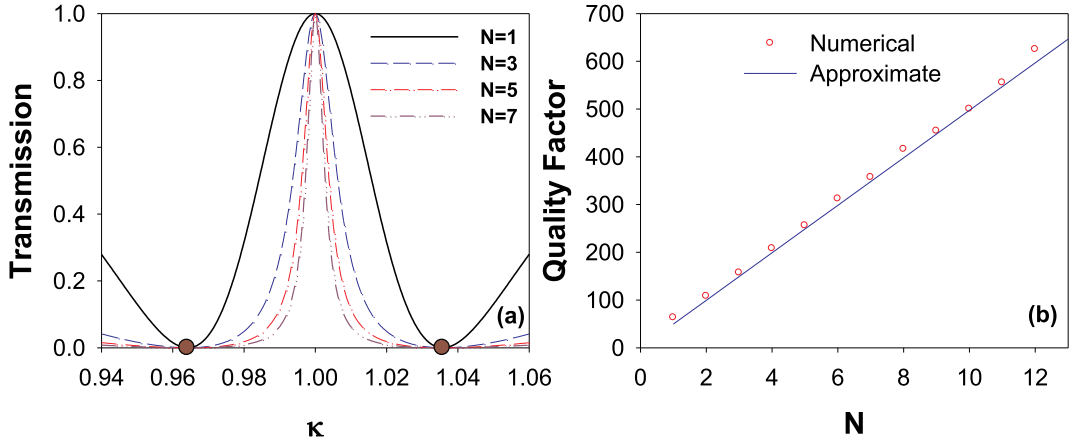

Fig. 11. (a) The same as in Fig. 10 (a) but for different values of N and f = 0.04. (b) Quality factor versus N. Solid lines and open circles correspond to numerical and approximate results respectively.

whatever the value of d_1.

The behaviors of the quality factor and Fano parameters are given in Fig. 13 (a) and (b) respectively. The quality factor (Fig. 13(a)) reaches its maximal value (≈200) for $d_1 = 0.5$ and decreases for d_1 far from this value. The Fano parameters q_{1t} and q_{2t} are opposite for $d_1 = 0.5$ (Eq. (27)), whereas for $d_1 \neq 0.5$, q_{1t} and q_{2t} are quite different showing clearly the asymmetric shape of the EIT resonances around $\kappa = 1$. All the above results show that the EIT resonance parameters can be tuned easily by varying the magnetic flux or by varying the length of the wire connecting the ring to the waveguide.

3.3. *Electromagnetic induced reflection*

As mentioned above (Figs. 4(b) and 6), it is possible to squeeze a reflection resonance between two reflection zeros (the so-called EIR resonance) for integers values of the length d_1 around $\kappa = 1$ and in presence of a magnetic flux. We plot in Fig. 14 the reflection spectra (in color scale) versus κ and d_1 for f = 0 (Fig. 14(a)) and f = 0.03 (Fig. 14 (b)). We have indicated by horizontal dashed line the position of BIC states in Fig. 14(a) for f = 0. These states are hidden and do not give any signature in the reflection spectra as the corresponding resonances have zero width (see Fig. 15). In particular, one can notice a decrease of the reflection from zero at $d_1 = 0.5$ to one at $d_1 = 1$ and back to zero at $d_1 = 1.5$. Indeed, when the BIC states hold (i.e., $S = 0$, $C = 1$), the reflection rate (Eq. (10)) becomes

$$R = N^2 S_1^2 / \left(4C_1^2 + N^2 S_1^2\right) \tag{33}$$

which shows that at the BIC states (i.e., $kd = n\pi$), the reflection rate depends strongly on the value of d_1 and oscillates between 0 and 1. The positions of full transparency and full reflection regions in Fig. 14(a) coincide with those in Fig. 4(a). By applying a weak magnetic flux f = 0.03 (Fig. 14(b)), a thin reflection window appears between two minima around $\kappa = 1$ and $d_1 = 1$. The width of this window increases when the magnetic flux increases as it will be explained below. Also, contrary to the case f = 0 (Fig. 14(a)), the reflection at $\kappa = 1$ and f≠0 (Fig. 14(b)) increases from zero at $d_1 = 0.5$ to one at $d_1 = 1$ and back to zero at$d_1 = 1.5$according to the equation

$$R = N^2 C_1^2 / \left(4S_1^2 + N^2 C_1^2\right) \tag{34}$$

Fig. 15 gives three examples of the reflection spectra versus κ with (blue curves) and without (red curves) magnetic flux for different values of d_1. Fig. 15(b) shows that for $d_1 = 1$ applying a magnetic flux induces a complete reflection of the incident wave through a very small energy window in accordance with Fig. 14 (b). For $d_1 = 0.8$ (Fig. 15(a)) or $d_1 = 1.2$ (Fig. 15 (c)) one obtains an asymmetric EIR resonance. This resonance is a consequence of the coupling between BIC states given by Eq. (18) and other states given by Eq. (19).

Similarly to the above study about symmetric and asymmetric EIT resonances, we have performed a detailed sudy for EIR resonances. In order to avoid redundancy and lighten the text, we give these results in Appendix B for a reader interested by the details of the calculations.

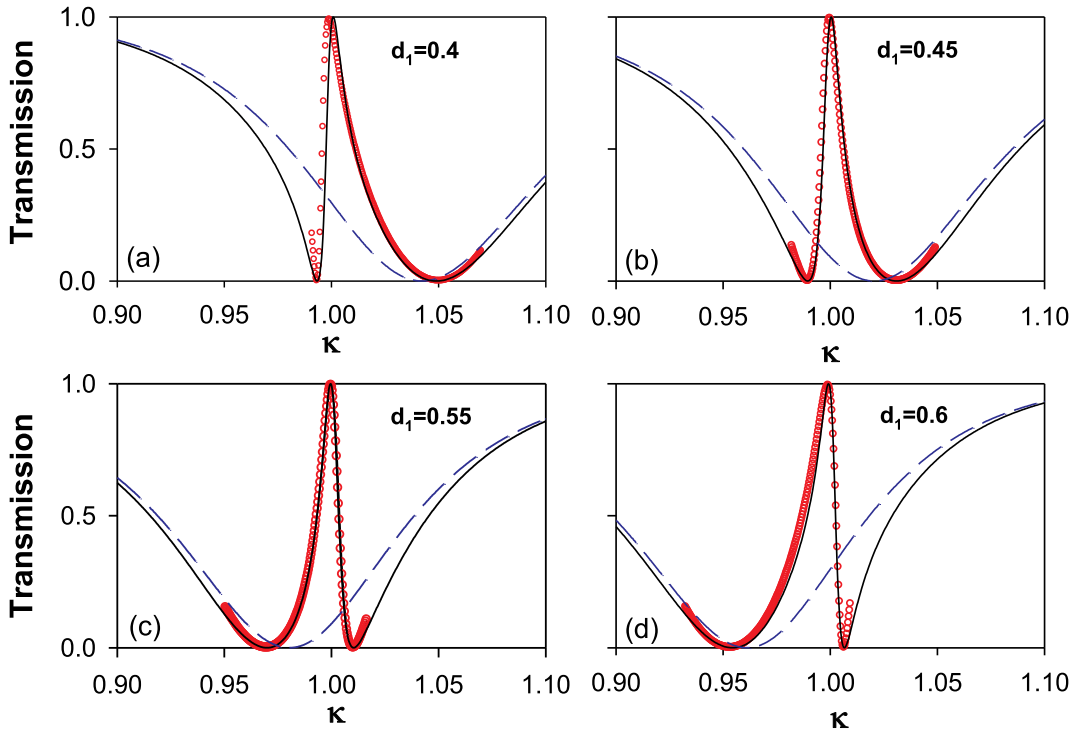

Fig. 12. Transmission cofficient versus the dimensionless wave vector κ for different values of d_1. Dashed and solide lines correspond to f = 0 and 0.02 respectively, red open cercles present the approximate results obtained by Taylor expansion around the resonance (κ = 1). (For interpretation of the references to color in this figure legend, the reader is referred to the Web version of this article.)

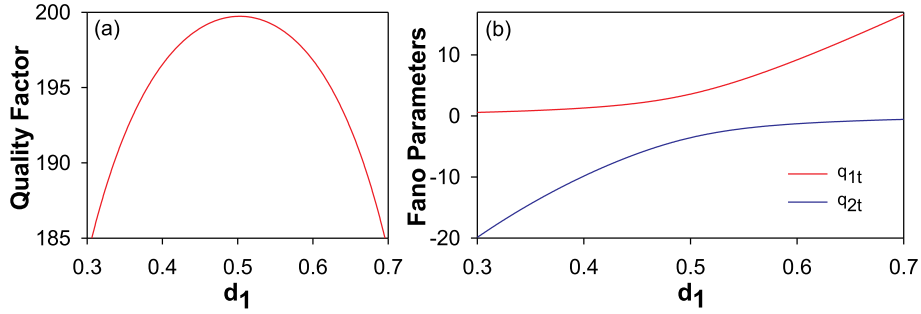

Fig. 13. (a) Theoretical variation of the quality factor Q_T of the transmission resonance. (b) Variation of the Fano parameters of the transmission resonance around $kd = \pi$ as a function of the length d_1 for f = 0.02.

4. Effect of temperature on EIT and EIR resonances

In all the above results, we have considered EIT and EIR resonances at zero temperature. In order to take account of the thermal effect, we should employ the Landauer-Büttiker formula [68,69] giving the finite temperature conductance from the transmission rate$T(E)$in one-dimensional channels as [33,34].

$$G_T\left(E_F,\theta\right) = G_0 \int dE\left(-\frac{\partial f(E,E_F,\theta)}{\partial E}\right) T\left(E\right) \tag{35}$$

where $G_0 = \frac{2e^2}{h}$is the quantum conductance, h the Planck constant and we have chosen θ to designate the temperature to be distinguished from the transmission T. $f(E)$ is the Fermi distribution function given by$f(E,E_F, \theta) = [e^{(E-E_F)/k_B\theta} + 1]^{-1}$where$E_F$is the Fermi energy and $k_B$the Boltzmann constant. By using the following change of variables $E = E^*\kappa^2$where $E^* = \frac{\hbar^2\pi^2}{2md^2}$ is the units of energy that enables to transform κ to$E$ and the dimensionless temperature$\theta_d = k_B\theta/E^*$, then Eq. (35) can be written as

$$G_T(\kappa_F,\theta) = \frac{G_0}{2\theta_d}\int d\kappa\ T(\kappa)\ \cosh^{-2}\left(\frac{\kappa^2-\kappa_F^2}{2\theta_d}\right) \tag{36}$$

It is worth mentioning that if we chose a small quantum ring of perimeter $L = 200\ nm$ (i.e., $d = 100\ nm$) and all the wires are made of GaAs semiconductor with effective electron mass $m = 0.067m_0$ ($m_0$is the free electron mass), then a temperature $\theta = 533\ mK$will correspond to $\theta_d = 0.1$. These parameters are connected to the experimental realizations [75,76]. Equation (36) has been used successfully to explain the temperature dependence of the A-B oscillations in a single mode ballistic ring [77]. Also, the temperature dependence of the Fano resonance in electronic transport of quantum wires and rings [78,79] with impurities has been addressed based on Eq. (36).

Fig. 16(a) and (b) give the normalized conductanceG_T/G_0versus the dimensionless Fermi wave vector $\kappa_F = (E_F/E^*)^{1/2}$for $d_1 = 0.5$and $d_1 = 1$at different temperatures respectively. The magnetic flux through the ring is fixed to f = 1.05 (i.e., a magnetic field B = 1.37 T [78]). One can see that the EIT and EIR resonances are considerably affected when the temperature increases, however the EIT (EIR) keep the shape of a

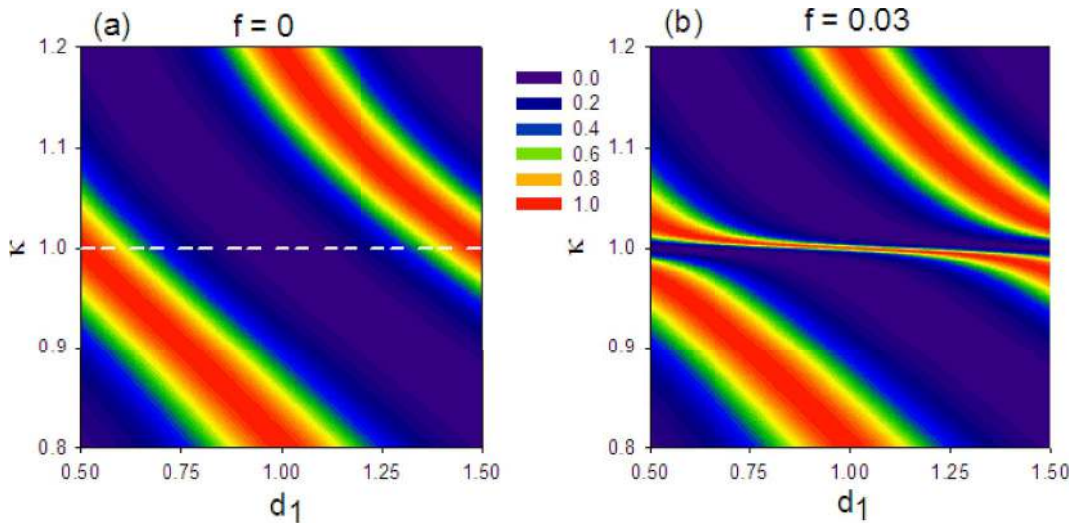

Fig. 14. (a) Reflection spectra (in color scale) versus the dimensionless wave vector κ and the length $d_1$for f = 0. (b) Same as in (a) but for f = 0.03. (For interpretation of the references to color in this figure legend, the reader is referred to the Web version of this article.)

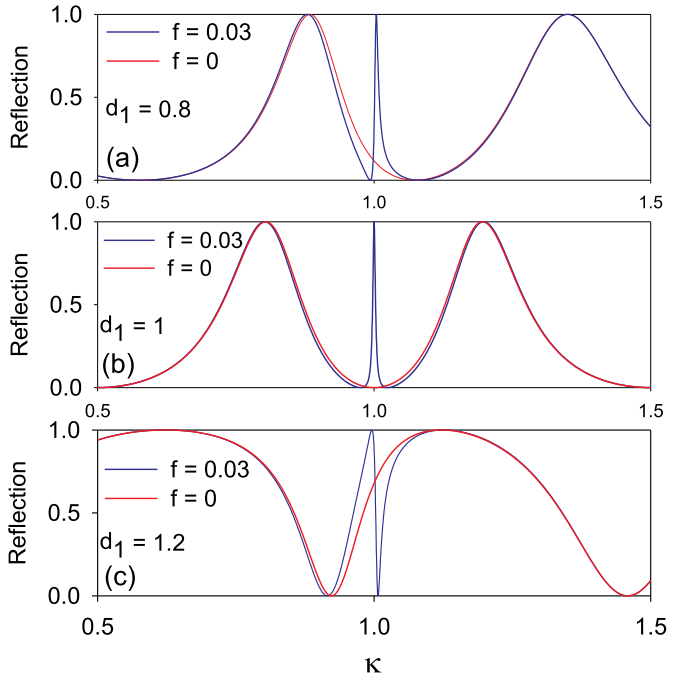

Fig. 15. Reflection cofficient versus the dimensionless wave vector κ for $d_1 = 0.8$ (a), 1 (b) and 1.2 (c). The red and blue curves are plotted for f = 0 and 0.03 respectively. (For interpretation of the references to color in this figure legend, the reader is referred to the Web version of this article.)

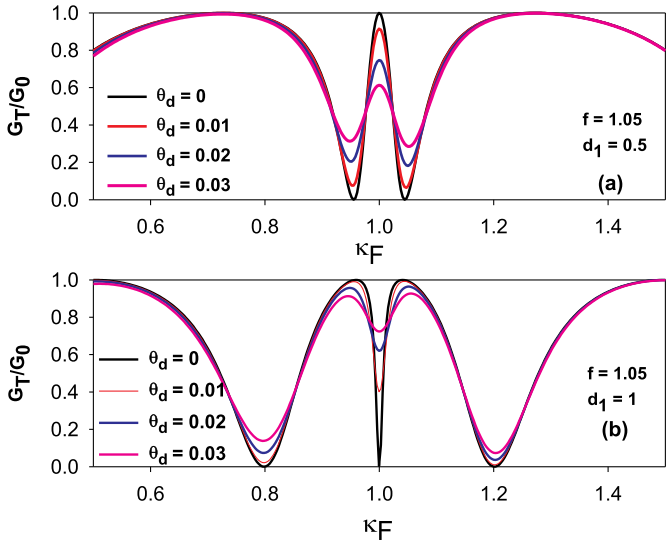

Fig. 16. (a) Normalized conductance versus the dimensionless Fermi wave vector κ_F for different temperatures for $d_1 = 0.5$ and f = 1.05. (b) Same as in (a) but for $d_1 = 1$.

resonance (dip) squeezed between two dips (resonances). Let us recall that $\theta_d = 0.01$corresponds to$\theta = 53.3\ mK$etc. The amplitudes of the resonances decrease, whereas the magnitudes of the dips increase when increasing the temperature. In particular, thinner resonances and anti-resonances are more affected by the temperature (Fig. 16(a), (b)). These results are summarized in Fig. 17 (a) and (b) where we can see that EIT resonance shape around $\kappa = 1$ceases to exist for $\theta_d > 0.05$ (Fig. 17(a)) whereas the EIR resonance shape ceases to exist for $\theta_d > 0.03$ (Fig. 17(b)).

5. Conclusion

In the present work, we have investigated theoretically and numerically the existence of EIT and EIR resonances in a simple mesoscopic structure composed of an Aharonov-Bohm ring of length 2d attached vertically to two semi-infinite leads (waveguide) by a wire of length d_1. The number of dangling wire-ring resonators attached at the same point is N. A general analytical expression for the transmission and reflection coefficients as well as dispersion relations are obtained by means of the Green's function method in the presence of a magnetic flux. The behavior of the EIT and EIR is analyzed as a function of several parameters such as the geometry of the structure and the magnetic flux. We have demonstrated analytically that for particular values of the magnetic flux Φ, and in particular in the absence of the magnetic field, the structure exhibits bound in continuum (BIC) states with zero width resonance in transmission and reflection spectra. These trapped states transform to EIT or EIR resonances for particular values of length d_1 in presence of a weak magnetic flux. In order to understand the behavior of all the scattering parameters around the EIT and EIR resonances, we have performed in addition to numerical calculation, the approximate expressions of the transmission and reflection coefficients by using Taylor expansion around EIT and EIR resonances respectively for

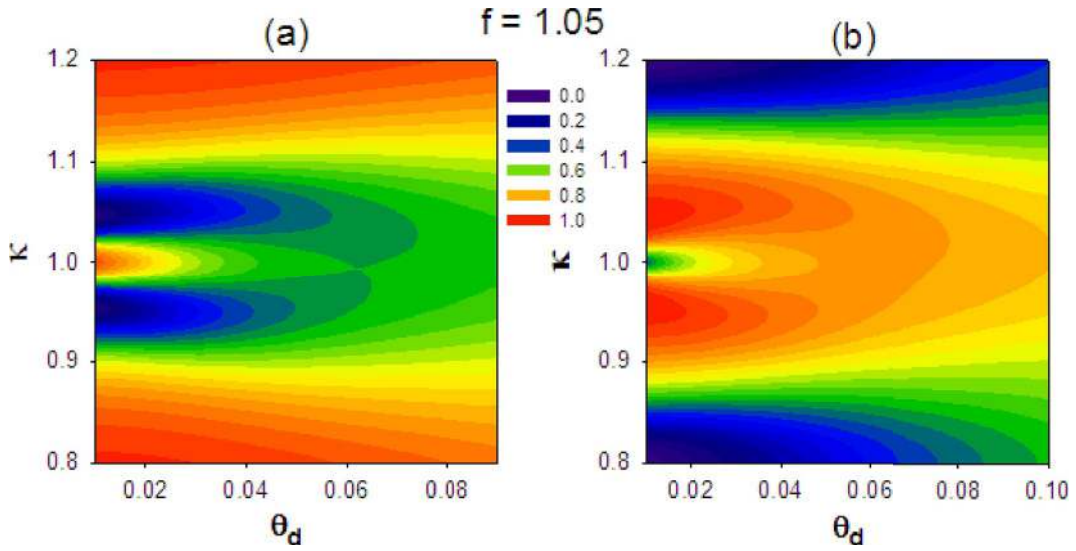

Fig. 17. (a) Normalized conductance versus the wave vector κ and temperature θ_d for $d_1 = 0.5$ and f = 1.05. (b) Same as in (a) but for $d_1 = 1$.

$d_1 = 0.5d$ and $d_1 = d$. In this context, we have shown a good agreement between numerical and approximate results. Also, we have deduced the Fano parameter q and the quality factor Q. The latter is analyzed as a function of the magnetic flux and the number of dangling resonators N. Indeed, it has been found that Q decreases as function of the magnetic flux f for both resonances, whereas it increases (decreases) as function of N for EIT (EIR) resonances. From the experimental point of view, while the fabrication of $N = 1$ ring would be easier, the case $N = 2$ does not seem to be much more difficult and even the extension to $N = 3$ or 4 should be feasible. The effect of temperature on EIT and EIR resonances is also considered through an analysis of the Landauer-Buttiker conductance formula. As predicted, the EIT resonance broadens and its intensity decreases when temperature increases. Similarly the dip (anti-resonnace) associated to the EIR resonance in the conductance broadens and its intensity increases versus temperature. The structure proposed in this work may have important applications for electronic transport in mesoscopic systems like filters and demultiplexers. The possibility to realize a Y-shaped demultiplexer [80] with one input line and two output lines; where each containing its own appropriate wire-ring resonator is in progress. Indeed, such as device would allow filtering a given energy in one line keeping the other line unaffected.

Appendix A. BIC, EIT and EIR resonances for $C' \approx 0$

The explicit expressions giving the eigenstates for DBC and NBC structures (Eqs. (13) and (14) can also be written respectively as

$$C\left[C + \frac{SC_1}{2S_1}\right] - C'^2 = 0 \tag{A1}$$

and

$$C\left[C - \frac{SS_1}{2C_1}\right] - C'^2 = 0 \tag{A2}$$

In presence of a magnetic flux such that$C' = 0$ (i.e., f is half integer), we obtain two types of eigenstates of the DBC structure (Eq. (A1)) which are totally decoupled from each other. These states are given by

$$C = 0 \tag{A3}$$

or

$$C + \frac{SC_1}{2S_1} = 0 \tag{A4}$$

They are respectively associated to the ring alone or to the ring-wire system alone. These two types of states coincide with each other for $C = 0$and $C_1 = 0$, i.e.,

$$d_1 / d = (2m+1)/(2n+1) \tag{A5}$$

where m and n are integers. Similarly, we obtain two types of eigenstates of the NBC structure (Eq. (A2)) totally decoupled from each other and given by

$$C = 0 \tag{A6}$$

or

$$C-\frac{SS_1}{2C_1}=0 \tag{A7}$$

These two types of states coincide with each other for $C = 0$and $S_1 = 0$, i.e.,

$$d_1 / d = m/(2n+1) \tag{A8}$$

Equation (A3) shows that the eigenstates of the DBC structure are the consequence of the coupling by means of the magnetic flux, between the states given by$C = 0$ of the ring alone (Fig. 2(b)) and those given by $C+\frac{SC_1}{2S_1}=0$ which are associated to the coupled ring-wire (Fig. 3(a)). Similarly, Eq. (45) shows that the eigenstates of the NBC structure are the consequence of the coupling between the states given by$C = 0$of the ring alone (Fig. 2(b)) and those given by $C-\frac{SS_1}{2C_1}=0$ of the coupled ring-wire (Fig. 3(b)). These results demonstrate that the eigenstates of DBC and NBC structures are the consequence of the coupling between two resonators by means of the magnetic flux such that $C' \neq 0$(i.e., f is non-half integer).

We can notice that the states given by $C = 0$are common to both structures (DBC and NBC). These states are independent of the wire of length d_1 and therefore they remain trapped in the ring even if the ring-wire structure is connected to the semi-infinite leads. Indeed, we can show easily that the eigenstates of the whole system (Fig. 1) are given by

$$C[2(C_1S+2S_1C)-jN(SS_1-2C_1C)]=0 \tag{A9}$$

Equation (A9) clearly shows that if

$$C=0 \tag{A10}$$

(i.e., $S = \pm 1$), then one obtains the BIC states of the whole system (Fig. 1). From Eq. (A10), BIC states are given by $kd = (2n + 1)\pi/2$ (n is an integer). The above results show that the BIC states are independent of the nature of the boundary condition at the bottom side of the ring-wire structure (Fig. 3), that is why they are common states to DBC and NBC structures and remain totally decoupled from the waveguide on which they are grafted.

In presence of a magnetic flux such that $C' \approx 0$(i.e., $f \approx l' + 1/2$ where l' is an integer), we can easily show that it is not possible to cancel simultaneously real and imaginary parts of Eq. (21) at the same energy, which means the impossibility of existence of BIC states. Also, as mentioned above, the eigenstates of the DBC structure (Eqs. (A3) and (A4)) and NBC structure (Eqs. (A6) and (A7)) for $f = l' + 1/2$ (half integer), become coupled when $f \approx l' + 1/2$ (see Eqs. (A1) and (A2)). This coupling between the eigenstates enables to transform the BIC states to either EIT or EIR resonances depending on the length d_1 of the wire in the same way as it was developed in this paper for the case where fis integer.

Appendix B. Symmetric and asymmetric EIR resonances

B.1. Case of symmetric EIR resonance

Similarly to the transmission coefficient, we give the approximate expression of the reflection function (Eq. (8)). A Taylor expansion in the vicinity of the reflection resonance around $kd = \pi + \varepsilon$ for $d_1 = 1$ enables us to write r as follows

$$r=jB\frac{\zeta_2\zeta'_2}{\varepsilon+jN\Delta^2/1+2\Delta^2} \tag{B1}$$

where $\zeta_2 = \varepsilon+\Delta\sqrt{2}/\sqrt{3+\Delta^2/2}$, $\zeta'_2=\varepsilon-(\Delta\sqrt{2}/\sqrt{3+\Delta^2/2})$ and $B = N(3+\Delta^2/2)/2(1+2\Delta^2)$. From the reflection coefficient (Eq. (B1)), one can show that the reflection rate R can be written following the Fano form [45]:

$$R=B^2\frac{(\varepsilon+q_2\Gamma_2)^2(\varepsilon-q_2\Gamma_2)^2}{\varepsilon^2+\Gamma_2^2} \tag{B2}$$

where $q_2 = \sqrt{2}(1+2\Delta^2)/N\Delta\sqrt{3+\Delta^2/2}$. The full width at half maximum of the EIR resonance falling at $\varepsilon = 0$ (i.e., $kd = \pi$), is given by

$$\Gamma_2=N\Delta^2/1+2\Delta^2 \tag{B3}$$

and therefore, the quality factor defined by $Q_2 = \pi/\Gamma_2$ is given by

$$Q_2=\pi\left(1+2\Delta^2\right)/N\Delta^2 \tag{B4}$$

We can notice thatq_2, $\Gamma_2$and Q_2 depend strongly on the magnetic flux f and the number of dangling resonators N. The results of the approximate expression (Eq. (B2)) are shown in Fig. B1 by open circles. These results are in accordance with the exact ones (solid lines) and clearly show that the resonance is an EIR-like resonance with $q_2 = 8.81$ and $2\Gamma_2 = 0.01745$. This resonance induced magnetically (Aharonov-Bohm effect) is squeezed between two reflection zeros (indicated by solid circles on the abscissa of Fig. B1) located symmetrically around $\kappa = 1$ and reaches unity (i.e., $R = 1$). The above calculation shows that a simple dangling ring, without introducing any impurity or defect in its arms, enables to obtain an EIR-like resonance with a width $2\Gamma_2$ and a coupling parameter$q_2$that can be tuned easily by varying the magnetic flux.

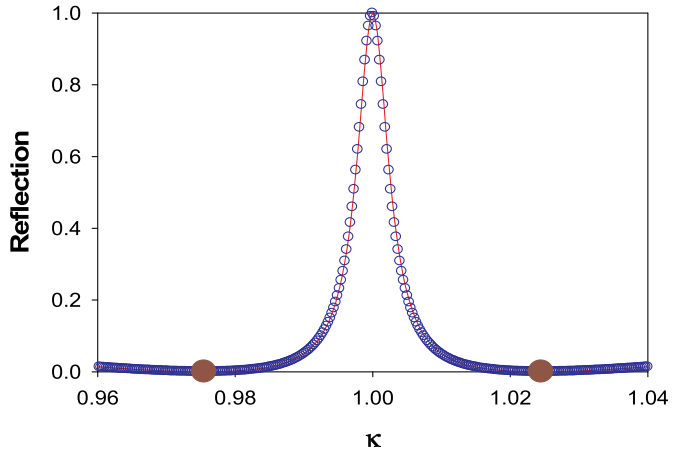

Fig. B1. Reflection spectrum versus κ (solid line) and the approximate results obtained by Taylor expansion (Eq. (B2)) (open circles) for the EIR resonance with $d_1 = 0.5$, $f = 0.03$ and $N = 1$.

The effect of the magnetic flux on electromagnetic induced reflection (EIR) is presented in Fig. B2(a). One can see that the width of the EIR resonance is very sensitive to the magnitude of the magnetic flux. Indeed, when the magnetic flux increases, the width of the EIR resonance decreases. In Fig. B2(b) we have plotted the approximate and numerical quality factor as a function of the magnetic flux. The approximate results (open circles) are in accordance with the exact ones (solid lines). On the other hand, the quality factor decreases when the flux increases and diverges when the flux vanishes. The insert of Fig. B2(b) shows the positions of the EIR resonance and reflection zeros as a function of the magnetic flux f. The slope of the two lines can be obtained easily from the reflection zeros of the approximate expression (Eq. (B2)) as $\pm\sqrt{2/3}$.

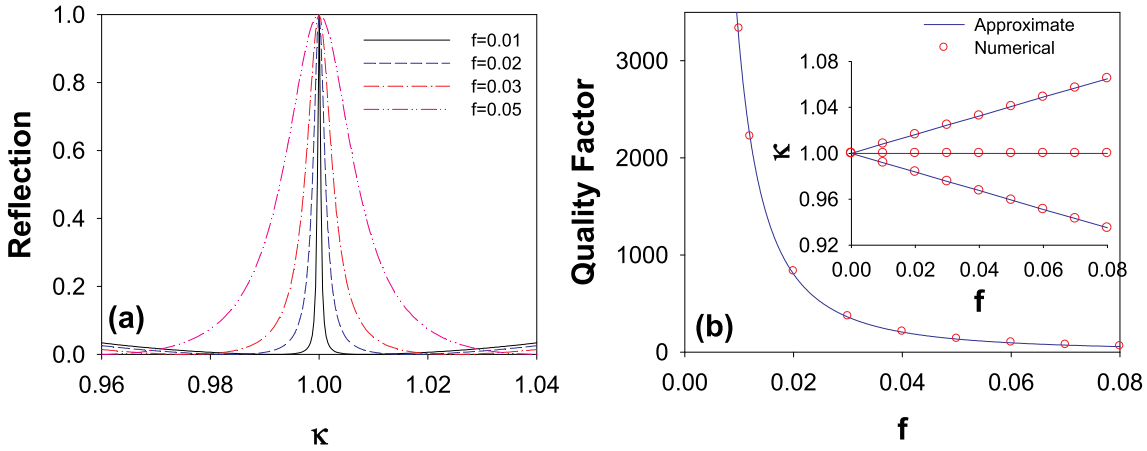

Fig. B2. (a) Same as in Fig. 15(b) around $\kappa = 1$ and for different values of the magnetic flux. (b) Quality factor versus the magnetic flux f. Solid lines and open circles correspond to numerical and approximate results respectively. The insert shows the variation of the positions of reflection zeros versus the magnetic flux f.

Figure B3(a) gives the reflection spectra versus κ for different values of N. The magnetic flux is fixed at $f = 0.02$. One can notice that, contrary to the EIT resonance (Fig. 11(a)), the width of the EIR increases when increasing N (Fig. B3(a)). These resonances remains squeezed between two transmission zeros located symmetrically around $\kappa = 1$ (indicted by solid circles on the abscissa) of Fig. B3(a). In Fig. B3(b), we have plotted the evolution of the quality factor as a function of $1/N$. This result shows that Q increases linearly as function of $1/N$ according to Eq. (B4), also a good agreement between approximate and numerical results has been achieved.

B.2. Case of asymmetric EIR resonance

As mentioned in Fig. 15, in order to show asymmetric EIR resonances, we have to take d_1 slightly different from d and in presence of a weak magnetic flux through the ring of length $2d$. However, in order to show that such resonances follow a Fano form, we have made a Taylor expansion of the expression of the reflection coefficient (Eq. (8)) around the EIR resonance at $kd = \pi$. After a tedious calculation, we found the following expression for the reflection rate

$$R = B^2 \frac{(\varepsilon + q_{r1}\Gamma_r)^2 (\varepsilon + q_{r2}\Gamma_r)^2}{\varepsilon(\varepsilon - \beta_r) + \Gamma_r^2} \tag{B5}$$

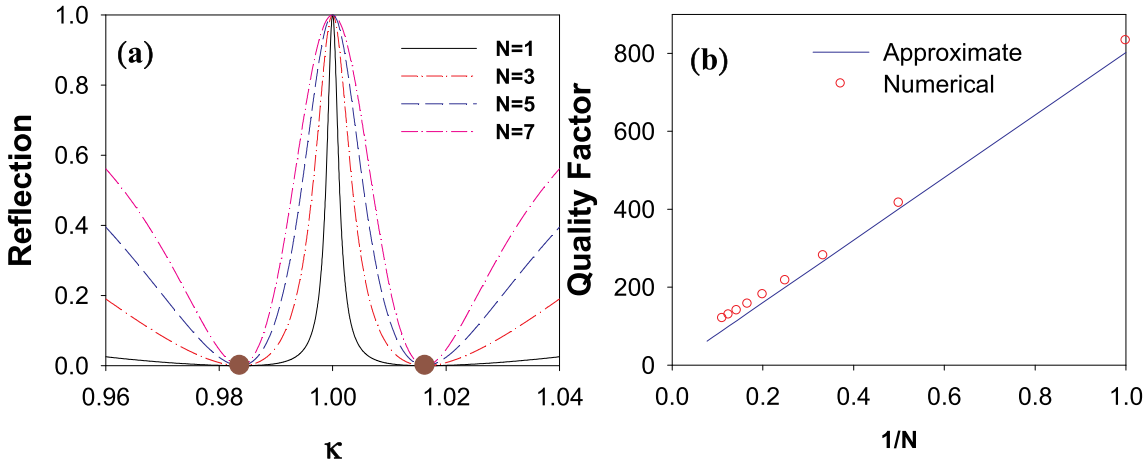

Fig. B3. (a) Same as in Fig. 17 (a) but for different values of N and f = 0.04. (b) Quality factor versus $1/N$. Solid lines and open circles correspond to numerical and approximate results respectively.

where B is constant. q_{1r} and q_{2r} are the Fano parameters that describe the asymmetry of the resonance. Contrary to the symmetrical case, q_{1r} and q_{2r} are different; their expressions are cumbersome, they depend on the geometrical parameters of the structure as well as on the magnetic flux applied through the ring. We shall avoid giving their expressions here. β_r gives the resonance position; its expression is given by

$$\beta_r = -\frac{2\Delta^2\phi(\phi^2-2)\left(N^2-4\right)}{4\left(2\Delta^2(1+\delta)+1-\frac{\phi^2}{2}\right)^2+N^2\phi^2(2\Delta^2(1+\delta)+1)^2} \tag{B6}$$

The full width at half maximum of the EIR asymmetric resonance falling at $\varepsilon = \beta_r$ is given by

$$\Gamma_r = \left(\frac{16\phi^2\Delta^4+N^2\Delta^4\left(\phi^2-2\right)^2}{4\left(2\Delta^2\left(1+\delta\right)+1-\frac{\phi^2}{2}\right)^2+N^2\phi^2\left(2\Delta^2\ \ 1+\delta\right)+1\Big)^2}\right)^{0.5} \tag{B7}$$

where $\Delta = \pi f$, $\phi = \pi\delta$ and $\delta = d_1$-d. Therefore, the quality factor can be deduced as $Q_R = \pi/\Gamma_r$.

The results of the approximate expression (Eq. (B5)) are shown in Fig. B4 by red open circles. These results are in accordance with the exact ones (solid lines) and clearly show that the resonance is an asymmetric EIR resonance. This resonance induced magnetically (Aharonov-Bohm effect) is squeezed between two transmission zeros located asymmetrically around κ = 1 and reaches unity (i.e., T = 1) whatever the value of d_1. The behaviors of the quality factor and Fano parameters are given in Figs. B5 (a) and (b) respectively. The quality factor (Fig. B5(a)) reaches its maximal value (≈800) for $d_1 = 1$ and decreases for d_1 far from this value. The Fano parameters q_{1r} and q_{2r} are opposite for $d_1 = 1$ (Eq. (B2)), whereas for $d_1 \neq 1$, q_{1t} and q_{2t} are quite different showing clearly the asymmetric shape of the EIT resonances around κ = 1. These two parameters give information on the degree of asymmetry of the resonance profile. We find that for values of d_1 less than 1, q_{1r} varies greatly while q_{2r} remains almost constant around 0 and the inverse happens when d_1 becomes greater than d. All the above results show that the EIR resonance parameters can be tuned easily by varying the magnetic flux or by varying the length of the wire connecting the ring to the waveguide.

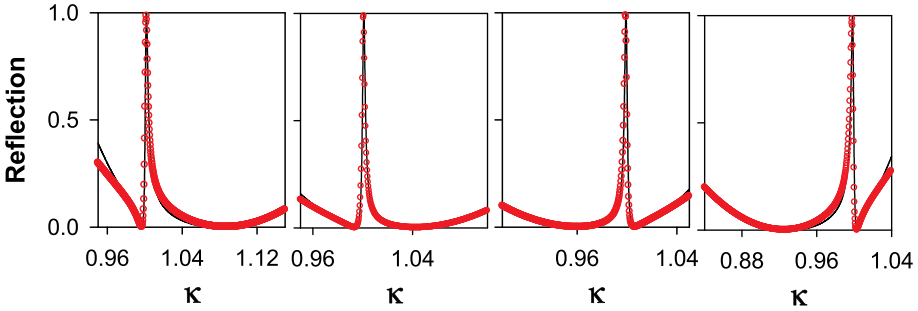

Fig. B4. Theoretical (solid line) variations of the reflection coefficient versus the dimensionless frequency κ for diffrents values of d_1, the magnetic flux is fixed to f = 0.02. The curves give a comparison between the approximate results obtained by Taylor expansion (red open circles) around the resonance with the exact calculations (solid lines).

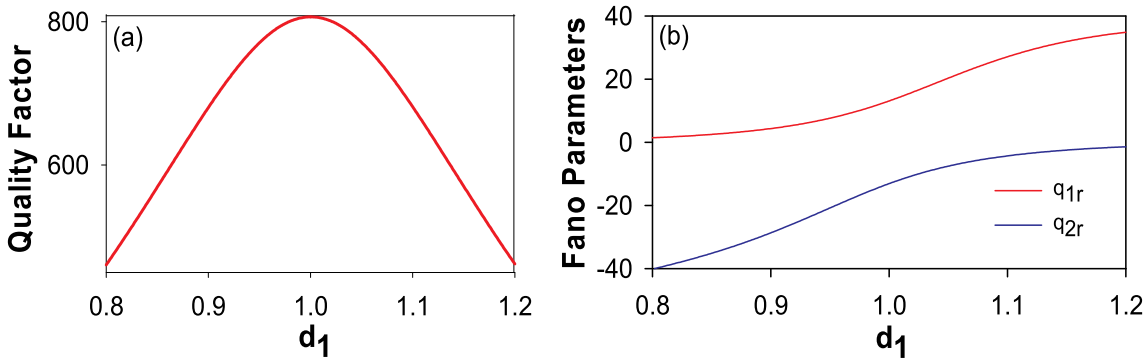

Fig. B5. Theoretical variation of the quality factor and Fano parameters of the asymmetric EIR around $kd = \pi$ as a function of the length d_1 for $f = 0.02$.

References

[1] K.J. Boller, A. Imamoglu, S.E. Harris, Phys. Rev. Lett. 66 (1991) 20.
[2] S. Harris, L. Hau, Phys. Rev. Lett. 82 (1999) 4611.
[3] K. Totsuka, N. Kobayashi, M. Tomita, Phys. Rev. Lett. 98 (2007) 213904.
[4] Y. Huang, C. Min, G. Veronis, Appl. Phys. Lett. 99 (2011) 143117.
[5] M. Manjappa, S.Y. Chiam, L.Q. Cong, A.A. Bettiol, W.L. Zhang, R. Singh, Appl. Phys. Lett. 106 (2015) 181101.
[6] M. Fleischhauer, A. Imamoglu, J.P. Marangos, Rev. Mod. Phys. 77 (2005) 633.
[7] S. Fan, J.D. Joannopoulos, Phys. Rev. B 65 (2002) 235112.
[8] X. Yang, M. Yu, D.L. Kwong, C.W. Wong, Phys. Rev. Lett. 102 (2009) 173902.
[9] Y. Sato, Y. Tanaka, J. Upham, Y. Takahashi, T. Asano, S. Noda, Nat. Photonics 6 (2012) 56.
[10] Q. Xu, S. Sandhu, M.L. Povinelli, J. Shakya, S. Fan, M. Lipson, Phys. Rev. Lett. 96 (2006) 123901.
[11] H.M. Li, S.B. Liu, S.Y. Liu, S.Y. Wang, H.F. Zhang, B.R. Bian, X.K. Kong, Appl. Phys. Lett. 106 (2015), 083511.
[12] S.C. Tian, R.G. Wan, E.B. Xing, J.M. Rong, H. Wu, L.J. Wang, et al., Physica E 69 (2015) 349.
[13] H. Hamedi, M.R. Mehmannavaz, Physica E 66 (2015) 309.
[14] R. Taubert, M. Hentshel, J. Kastel, H. Giessen, Nano Lett. 12 (2012) 136.
[15] T. Liu, H. Wang, Y. Liu, L. Xiao, C. Zhou, C. Xu, S. Xiao, Physica E 104 (2018) 229.
[16] E.H. El Boudouti, T. Mrabti, H. Al-Wahsh, B. Djafari-Rouhani, A. Akjouj, L. Dobrzynski J. Phys, Condens. Matter 20 (2008) 255212.
[17] A. Santillan, S.I. Bozhevolnyi, Phys. Rev. B 84 (2011), 064304.
[18] A. Merkel, G. Theocharis, O. Richoux, V. Romero-Garcìa, V. Pagneux, Appl. Phys. Lett. 107 (2015) 244102.
[19] I. Quotane, E.H. El Boudouti, B. Djafari-Rouhani, Phys. Rev. B 97 (2018), 024304.
[20] A. Mouadili, E.H. El Boudouti, A. Soltani, A. Talbi, A. Akjouj, B. Djafari-Rouhani, J. Appl. Phys. 113 (2013) 164101.
[21] A. Mouadili, E.H. El Boudouti, A. Soltani, A. Talbi, B. Djafari- Rouhani, A. Akjouj, K. Haddadi, J. Phys. Condens. Matter 26 (2014) 505901.
[22] J. Jiang, Q. Zhang, Q. Ma, S. Yan, F. Wu, X. He, Opt. Express 5 (2015) 1962.
[23] X. He, Y. Yao, Y. Huang, Q. Zhang, L. Zhu, F. Wu, G. Ying, J. Jiang, Opt. Commun. 407 (2018) 386.
[24] D. Chun-Feng, Z. Ya-Ting, Y. Jian-Quan, S. Chong-Ling, X.D. Gang, Z. Gui-Zhong, Chin. Phys. B 23 (2014) 124203.
[25] Z. Vafapour, A. Zakery, Plasmonics 11 (2016) 609.
[26] N. Liu, T. Weiss, M. Mesch, L. Langguth, U. Eigenthaler, M. Hirscher, C. Sonnichsen, H. Giessen, Nano Lett. 10 (2010) 1103.
[27] S. Asgari, N. Granpayeh, J. Nanophotonics 11 (2017), 026012.
[28] S.F. Mingaleev, A.E. Miroshnichenko, Y.S. Kivshar, Opt. Express 16 (2008) 11647.
[29] H.J. Li, X. Zhai, L.L. Wang, Appl. Phys. Express 8 (2015), 092201.
[30] Y. Liu, Y.Q. Zhang, X.R. Jin, S. Zhang, Y.P. Lee, Opt. Commun. 371 (2016) 173.
[31] C.W. Hsu, B. Zhen, A.D. Stone, J.D. Joannopoulos, M. Soljacic, Nat. Rev. Mater 1 (2016) 16048.
[32] J. Von Neuman, E. Wigner, Phys. Z. 30 (1929) 465.
[33] S. Datta, Electronic Transport in Mesoscopic Systems, Cambridge University Press, Cambridge, 1995.
[34] Y. Imry, Introduction to Mesoscopic Physics, Oxford University Press, 1997.
[35] Y. Aharonov, D. Bohm, Phys. Rev. 115 (1959) 485. R. G. Chambers, Phys. Rev. Lett. 5, 3 (1960).
[36] M. Peshkin, A. Tonomura, The Aharonov-Bohm Effect, Lecture Notes in Physics, Springer, 1989.
[37] See the review by Tonomura, Proc. Jpn. Acad. Ser. 82 (2006) 45.
[38] V.G. Kravets, V G, et al., Nat. Mater. 12 (2013) 304.
[39] H. Vazquez, et al., Nat. Nanotechnol. 7 (2012) 663.
[40] A. Bachtold, et al., Nature 397 (1999) 673.
[41] S. Zaric, G.N. Ostojic, J. Kono, J. Shaver, V.C. Moore, M.S. Strano, R.H. Hauge, R. E. Smalley, X. Wei, Science 304 (2004) 1129.
[42] K. Fang, Z. Yu, S. Fan, Phys. Rev. Lett. 108 (2012) 153901.
[43] K. Fang, Z. Yu, S. Fan, Phys. Rev. B 87 (2013), 060301(R).
[44] E. Li, B.J. Eggleton, K. Fang, S. Fan, Nat. Commun. 5 (2014) 3225.
[45] U. Fano, Phys. Rev. 124 (1961) 1866.
[46] A.E. Miroshnichenko, S. Flach, Y.S. Kivshar, Rev. Mod. Phys. 82 (2010) 2257.
[47] K. Kobayashi, H. Aikawa, S. Katsumoto, Y. Iye, Phys. Rev. Lett. 88 (2002) 256806.
[48] J. Göres, D. Goldhaber-Gordon, S. Heemeyer, M.A. Kastner, H. Shtrikman, D. Mahalu, U. Meirav, Phys. Rev. B 62 (2000) 2188.
[49] M.L. Ladrón de Guevara, F. Claro, P.A. Orellana, Phys. Rev. B 67 (2003) 195335.
[50] A.C. Johnson, C.M. Marcus, M.P. Hanson, A.C. Gossard, Phys. Rev. Lett. 93 (2004) 106803.
[51] M.A. Kokoreva, V.A. Margulis, M.A. Pyataev, Physica E 43 (2011) 1610.
[52] K. Kobayashi, H. Aikawa, S. Katsumoto, Y. Iye, Physica E 22 (2004) 468.
[53] V. Vargiamidis, H.M. Polatoglou, Phys. Rev. B 74 (2006) 235323.
[54] H. Lu, R. Lü, B.F. Zhu, Phys. Rev. B 71 (2005) 235320.
[55] X.-Q. Wang, S.-F. Zhang, C. Jiang, G.Y. Yi, W.-J. Gong, Physica E 104 (2018) 1.
[56] K. Kang, Phys. Rev. B 59 (1999) 4608.
[57] H. Al-Wahsh, E.H. El Boudouti, B. Djafari-Rouhani, A. Akjouj, L. Dobrzynski, Phys. Rev. B 75 (2007) 125313.
[58] J. Yi, J.H. Wei, J. Hong, S.I. Lee, Phys. Rev. B 65 (2001), 033305.
[59] W.J. Hsueh, R.Z. Qiu, C.H. Chen, Eur. Phys. J. B 86 (2013) 27.
[60] W.J. Hua, C.Y. Xue, X.S. Jie, M.L. Mo, H. Jongbae, Commun. Theor. Phys. 39 (2003) 3.
[61] G.Y. Fang, Z.Y. Ping, L.J. Qing, Chin. Phys. 14 (2005) 196.
[62] C. Jiang, Y.S. Zheng, Solid State Commun. 212 (2015) 14.
[63] S.K. Maiti, Phys. Lett. A 373 (2009) 4470.
[64] P. Dutta, S.K. Maiti, S.N. Karmakar, Solid State Commun. 150 (2010) 1056.
[65] T. Mrabti, Z. Labdouti, O. El Abouti, E.H. El Boudouti, F. Fethi, B. Djafari-Rouhani, Phys. Lett. A 382 (2018) 613.
[66] P.A. Orellana, M. Pacheco, Phys. Rev. B 71 (2005) 235330.
[67] R. Akis, P. Vasilopoulos, P. Debray, Phys. Rev. B 56 (1997) 9594.
[68] R. Landauer, IBM J. Res. Dev. 1 (1957) 233.
[69] M. Büttiker, Phys. Rev. B 38 (1988) 9375.
[70] L. Dobrzynski, E.H. El Boudouti, A. Akjouj, Y. Pennec, H. Al-Wahsh, G. Lévêque, B. Djafari- Rouhani, Phononics, Elsevier, 2017.
[71] Y. El Hassouani, H. Aynaou, E.H. El Boudouti, B. Djafari-Rouhani, A. Akjouj, V. R. Velasco, Phys. Rev. B 74 (2006), 035314.
[72] E.H. El Boudouti, Y. El Hassouani, B. Djafari-Rouhani, H. Aynaou, Phys. Rev. E 76 (2007), 026607.
[73] F. Liu, M. Ke, A. Zhang, W. Wen, J. Shi, Z. Liu, P. Sheng, Phys. Rev. E 82 (2010), 026601.
[74] X. Liu, J. Gu, R. Singh, Y. Ma, J. Zhu, Z. Tian, M. He, J. Han, W. Zhang, Appl. Phys. Lett. 100 (2012) 131101.
[75] I.G. Zacharia, D. Goldhaber-Gordon, G. Granger, M.A. Kastner, Yu B. Khavin, H. Shtrikman, D. Mahalu, U. Meirav, Phys. Rev. B 64 (2001) 155311.
[76] U.F. Keyser, C. Fühner, S. Borck, R.J. Haug, M. Bichler, G. Abstreiter, W. Wegscheider, Phys. Rev. Lett. 90 (2003) 196601.
[77] M. Cassé, Z.D. Kvon, G.M. Gusev, E.B. Olshanetskii, L.V. Litvin, A.V. Plotnikov, D. K. Maude, J.C. Portal, Phys. Rev. B 62 (2000) 2624.
[78] V. Vargiamidis, H.M. Polatoglou, Phys. Rev. B 75 (2007) 153308, ibid 74, 235323 (2006).
[79] V. Vargiamidis, V. Fessatidis, in: B. Ekwall, M. Cronquist (Eds.), Micro Electro Mechanical Systems, Nova Science Publishers, Inc., 2010.
[80] A. Mouadili, E.H. El Boudouti, A. Soltani, A. Talbi, K. Haddadi, A. Akjouj, B. Djafari-Rouhani, J. Phys. D Appl. Phys. 52 (2019), 075101.